

Piezoelectric quantum spin Hall insulator with Rashba spin splitting in Janus monolayer SrAlGaSe₄

San-Dong Guo¹ Yu-Tong Zhu¹, Wen-Qi Mu¹ and Xing-Qiu Chen^{2,3}

¹*School of Electronic Engineering, Xi'an University of Posts and Telecommunications, Xi'an 710121, China*

²*Shenyang National Laboratory for Materials Science, Institute of Metal Research, Chinese Academy of Science, 110016 Shenyang, Liaoning, P. R. China and*

³*School of Materials Science and Engineering, University of Science and Technology of China, Shenyang 110016, P. R. China*

The realization of multifunctional two-dimensional (2D) materials is fundamentally intriguing, such as combination of piezoelectricity with topological insulating phase or ferromagnetism. In this work, a Janus monolayer SrAlGaSe₄ is built from 2D MA₂Z₄ family with dynamic, mechanical and thermal stabilities, which is piezoelectric due to lacking inversion symmetry. The unstrained SrAlGaSe₄ monolayer is a narrow gap normal insulator (NI) with spin orbital coupling (SOC). However, the NI to topological insulator (TI) phase transition can be induced by the biaxial strain, and a piezoelectric quantum spin Hall insulator (PQSHI) can be achieved. More excitingly, the phase transformation point is only about 1.01 tensile strain, and nontrivial band topology can hold until considered 1.16 tensile strain. Moreover, a Rashba spin splitting in the conduction bands can exit in PQSHI due to the absence of a horizontal mirror symmetry and the presence of SOC. For monolayer SrAlGaSe₄, both in-plane and much weak out-of-plane piezoelectric polarizations can be induced with a uniaxial strain applied. The calculated piezoelectric strain coefficients d_{11} and d_{31} of monolayer SrAlGaSe₄ are -1.865 pm/V and -0.068 pm/V at 1.06 tensile strain as a representative TI. In fact, many PQSHIs can be realized from 2D MA₂Z₄ family. To confirm that, similar to SrAlGaSe₄, the coexistence of piezoelectricity and topological orders can be realized by strain (about 1.04 tensile strain) in the CaAlGaSe₄ monolayer. Our works suggest that Janus monolayer SrAlGaSe₄ is a pure 2D system for PQSHI, enabling future studies exploring the interplay between piezoelectricity and topological orders, which can lead to novel applications in electronics and spintronics.

PACS numbers: 71.20.-b, 77.65.-j, 72.15.Jf, 78.67.-n

Email:sandongyuwang@163.com

Keywords: Piezoelectricity, Topological insulator, Strain, Janus structure

I. INTRODUCTION

The multifunctional 2D materials can provide a unique opportunity for intriguing physics and practical device applications. The combination of piezoelectricity and ferromagnetism is one such example, which has been predicted in 2D vanadium dichalcogenides and septuple-atomic-layer VSi₂P₄^{1,2}. Other example is ferroelastic TI or ferroelectric TI, which simultaneously possesses ferroelastic or ferroelectric and quantum spin Hall (QSH) characteristics. The 2D Janus TMD MSSe (M = Mo and W) monolayers have been predicted as ferroelastic TI³, and the In₂Te₃/In₂Se₃ bilayer heterostructure as ferroelectric TI⁴. Antiferromagnetic TI with coexistence of intrinsic antiferromagnetism and QSH states also has been reported in XMnY (X=Sr and Ba; Y=Sn and Pb) quintuple layers⁵, as promising candidates for innovative spintronics applications. Piezoelectricity and band topology are two extensively studied distinct properties of insulators, and their coexistence in a single 2D material may lead to novel physical phenomenon and device applications.

The piezoelectric 2D semiconducting material, allowing for energy conversion between electrical and mechanical energy, has been a research focus in the ever-increasing energy conversion area^{6,7}. A 2D semiconducting material can show piezoelectric properties, when inversion symmetry is broken. A typical 2D piezoelec-

tric material is monolayer MoS₂ with 2H phase, which is firstly predicted by the first principles calculations⁸, and then is confirmed in experiment^{9,10}. In theory, many 2D monolayers are predicted as potential 2D piezoelectric materials by density functional theory (DFT) calculations^{2,8,11-18}. Piezoelectricity can be related with valley chern number in inhomogeneous hexagonal 2D crystals¹⁹, and nonlinear exciton drift in piezoelectric 2D materials has also been reported²⁰.

For TI with spin-momentum-locked conducting edge states and insulating properties in the bulk, the charge and spin transport in the edge states are quantized dissipationless, endowing them with rich physics and promising applications in spintronics and quantum computations^{21,22}. A 2D TI is also called as QSH insulator (QSHI) for its quantized edge conductance, and graphene is the first predicted 2D TI characterized by counter-propagating edge currents with opposite spin polarization²³. Experimentally, the HgTe/CdTe and InAs/GaSb quantum wells have been confirmed as QSHIs^{24,25}, and lots of QSHIs have also been theoretically proposed by DFT calculations²⁶⁻³¹.

Coexistence of intrinsic piezoelectricity and nontrivial band topology has been predicted in monolayer InXO (X=Se and Te) from our previous works³². However, the InXO (X=Se and Te) monolayers are built from monolayer InX (X=Se and Te) by oxygen functionalization with chemisorption of oxygen atoms on both sides. It may be more practical to search for pure

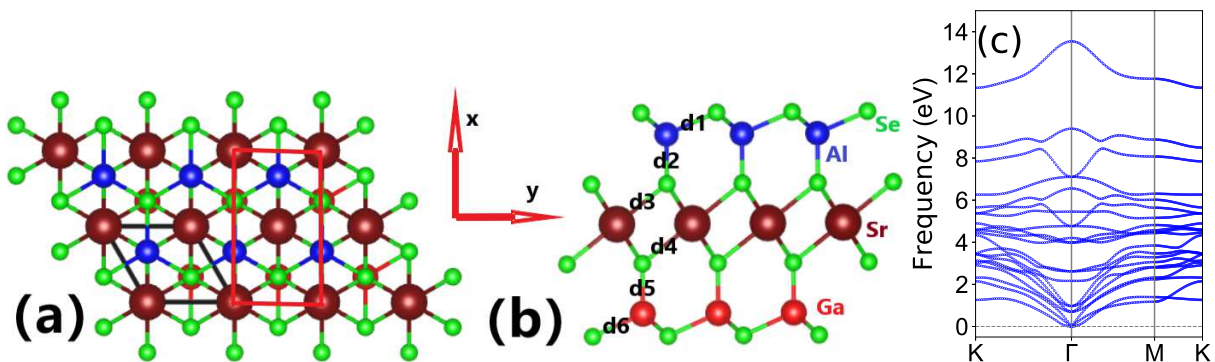


FIG. 1. (Color online) The (a) top view and (b) side view of crystal structure of monolayer SrAlGaSe_4 , and the rhombus primitive cell and rectangle supercell are marked by black and red frames, along with bond lengths d_i . (c) The phonon band dispersions of SrAlGaSe_4 monolayer by using GGA.

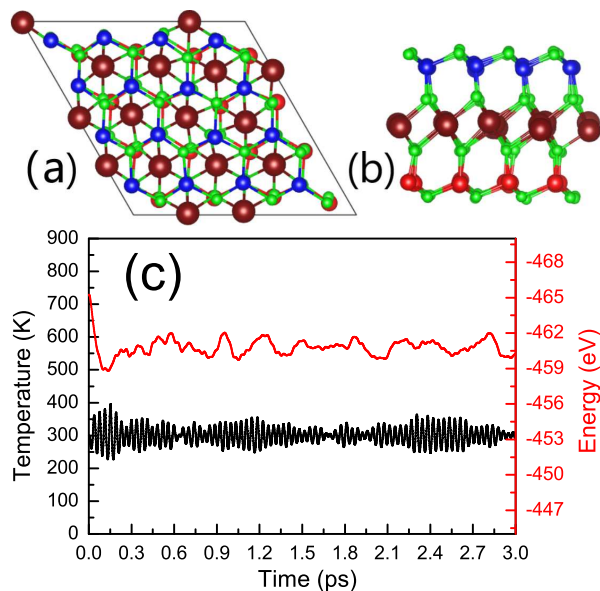


FIG. 2. (Color online) The (a) top view and (b) side view of crystal structures of SrAlGaSe_4 monolayer after the simulation for 3 ps at 300 K. (c) the temperature and total energy fluctuations of SrAlGaSe_4 monolayer at 300 K.

PQSHI, which can easily be confirmed in experiment. Recently, the 2D MA_2Z_4 family has attracted a surge of interest^{15,17,33–38}, and the MoSi_2N_4 and WSi_2N_4 monolayers are successfully synthesized by chemical vapor deposition (CVD)³³. Intrinsic piezoelectricity has been found in MA_2Z_4 family^{2,15,17}, such as α_1 - MoSi_2N_4 and WSi_2N_4 . On the other hand, β_2 - SrGa_2Se_4 is predicted to be a 2D TI with generalized gradient approximation (GGA)³⁴. It's a natural idea to achieve PQSHI in the new septuple-atomic-layer 2D MA_2Z_4 family.

In this work, we propose a design principle for the realization of PQSHI in 2D MA_2Z_4 family. Firstly, we chose a 2D TI β_2 - SrGa_2Se_4 from MA_2Z_4 family, which is centrosymmetric, lacking piezoelectricity. Secondly, to realize piezoelectric response, the inversion symmetry is bro-

TABLE I. For monolayer SrAlGaSe_4 , the lattice constants a_0 (Å), the bond lengths d_i (Å), the elastic constants C_{ij} (Nm^{-1}), shear modulus G_{2D} (Nm^{-1}), Young's modulus C_{2D} (Nm^{-1}), Poisson's ratio ν , the GGA and GGA+SOC gaps (meV).

a_0	d_1	d_2	d_3	d_4	d_5	d_6
4.07	2.56	2.30	3.00	2.99	2.33	2.58
C_{11}	C_{12}	G_{2D}	C_{2D}	ν	Gap	Gap _{SOC}
82.67	30.14	26.27	71.68	0.37	89.8	12.9

ken by constricting Janus SrAlGaSe_4 monolayer, which can be attained by replacing the Ga atoms of top GaSe bilayer in SrGa_2Se_4 monolayer with Al atoms. Finally, the biaxial strain is used to tune the topological properties of SrAlGaSe_4 monolayer. The Z_2 topological invariant is used to recognize the nontrivial topological state. Interestingly, by very small strain (about 1.01 tensile strain), the SrAlGaSe_4 monolayer can become PQSHI with additional Rashba spin splitting. To further confirm our design principle, similar to SrAlGaSe_4 , the PQSHI can be realized in the CaAlGaSe_4 monolayer by about 1.04 tensile strain. Therefore, the coupling between topological state and piezoelectricity is identified, offering a kind of new multifunctional 2D materials for novel designs in spintronics or optoelectronics.

The rest of the paper is organized as follows. In the next section, we shall give our computational details and methods. In the next few sections, we shall present crystal structure and stability, electronic structures and piezoelectric properties of Janus monolayer SrAlGaSe_4 . Finally, we shall give our discussion and conclusions.

II. COMPUTATIONAL DETAIL

Within DFT³⁹, the first-principles calculations are carried out using the projected augmented wave (PAW) method, as implemented in the VASP package^{40–42}. The

total energy convergence criterion is set to 10^{-8} eV with the cutoff energy for plane-wave expansion being 500 eV. We use GGA of Perdew, Burke and Ernzerhof (GGA-PBE)⁴³ as the exchange-correlation potential, and the SOC is considered to investigate electronic structures and piezoelectric stress coefficients e_{ij} . A Monkhorst-Pack mesh of $16 \times 16 \times 1$ is adopted for geometry optimization with the residual force on each atom being less than $0.0001 \text{ eV} \cdot \text{\AA}^{-1}$. The vacuum region along the z direction is set to more than 20 \AA in order to decouple the spurious interaction between the layers. The constant energy contour plots of the spin texture are calculated by the PYPROCAR code⁴⁴.

The Phonopy code⁴⁵ is used to calculate phonon dispersion spectrums of studied monolayers with a supercell of $5 \times 5 \times 1$ by finite displacement method. A $2 \times 2 \times 1$ k-mesh is employed with kinetic energy cutoff of 500 eV to calculate the second order interatomic force constants (IFCs). To obtain the piezoelectric strain coefficients d_{ij} , the elastic stiffness tensor C_{ij} and piezoelectric stress coefficients e_{ij} are calculated by using strain-stress relationship (SSR) and density functional perturbation theory (DFPT) method⁴⁶. The 2D elastic coefficients C_{ij}^{2D} and piezoelectric stress coefficients e_{ij}^{2D} have been renormalized by the length of unit cell along z direction (Lz): $C_{ij}^{2D} = Lz C_{ij}^{3D}$ and $e_{ij}^{2D} = Lz e_{ij}^{3D}$. A Monkhorst-Pack mesh of $16 \times 16 \times 1$ is adopted to calculate C_{ij} by GGA, and $5 \times 10 \times 1$ for e_{ij} by GGA+SOC. A tight-binding Hamiltonian with the maximally localized Wannier functions is constructed to fit band structures from the first-principles calculations, and then the Z_2 invariants are calculated, as implemented in the Wannier90 and WannierTools codes^{47,48}.

III. CRYSTAL STRUCTURE AND STABILITY

With SrSe₂ triple layers sandwiched between the GaSe bilayers, the septuple-atomic-layer SrGa₂Se₄ can be built with centrosymmetry and vertical reflection symmetry³⁴, which has disappeared piezoelectricity. To stimulate piezoelectricity, a natural way is to construct Janus structure, which can be achieved by replacing the Ga atoms of top GaSe bilayer in SrGa₂Se₄ monolayer with Al atoms, namely SrAlGaSe₄ monolayer. The symmetry space group of Janus monolayer SrAlGaSe₄ is reduced to No.156 from No.164 of SrGa₂Se₄ monolayer, which can induce both in-plane and out-of-plane piezoelectricity. The geometric structure of SrAlGaSe₄ monolayer is shown in Figure 1, along with both rhombus primitive cell and rectangle supercell. With armchair and zigzag directions defined as x and y directions, the rectangle supercell can be used to calculate piezoelectric coefficients e_{ij} . The optimized lattice constant of the Janus SrAlGaSe₄ monolayer is 4.07 \AA , and the interval distance between the upper Se layer and the lower Se layer is 10.38 \AA . In SrGa₂Se₄ monolayer, the equivalent bond lengths between d_1 and d_6 , or d_2 and d_5 , or d_3 and d_4 can be

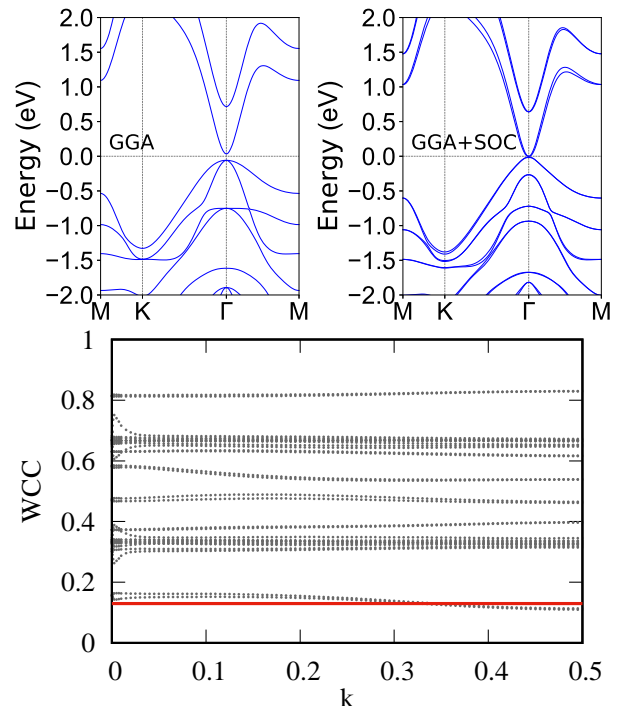


FIG. 3. (Color online) Top: The energy band structures of SrAlGaSe₄ monolayer using GGA and GGA+SOC. Bottom: Evolution of WCC of SrAlGaSe₄ monolayer at unstrained condition

observed. For monolayer SrAlGaSe₄, the difference in atomic sizes and electronegativities of Al and Ga atoms leads to inequivalent bond lengths and bond characteristics, which can be observed from Table I. The inequivalent bond lengths and bond characteristics can induce an electrostatic potential gradient, and then built-in electric field can be attained, which can give rise to Rashba spin splitting.

To study the stability of Janus SrAlGaSe₄ monolayer, we firstly calculate the phonon dispersion to validate its dynamic stability. As plotted in Figure 1, there is no imaginary vibrational frequency with three acoustic and eighteen optical phonon branches, which clearly suggests that SrAlGaSe₄ monolayer is dynamically stable. Moreover, both linear and flexural modes occur around the Γ point, which can be observed in most 2D materials^{34,49,50}. In addition, by performing ab-initio molecular dynamics (AIMD) simulations, we examine the thermal stability of SrAlGaSe₄ monolayer with a supercell of $4 \times 4 \times 1$ for more than 3000 fs at 300 K. The temperature and total energy fluctuations of SrAlGaSe₄ monolayer as a function of simulation time are plotted in Figure 2, along with the crystal structures of SrAlGaSe₄ at 300 K after the simulation for 3 ps. It is found that monolayer SrAlGaSe₄ undergoes no structural reconstruction with small temperature and total energy fluctuates around 300 K, which indicates the thermal stability of SrAlGaSe₄ monolayer.

To further check the mechanical stability of SrAlGaSe₄ monolayer, the elastic constants C_{ij} are calculated. Us-

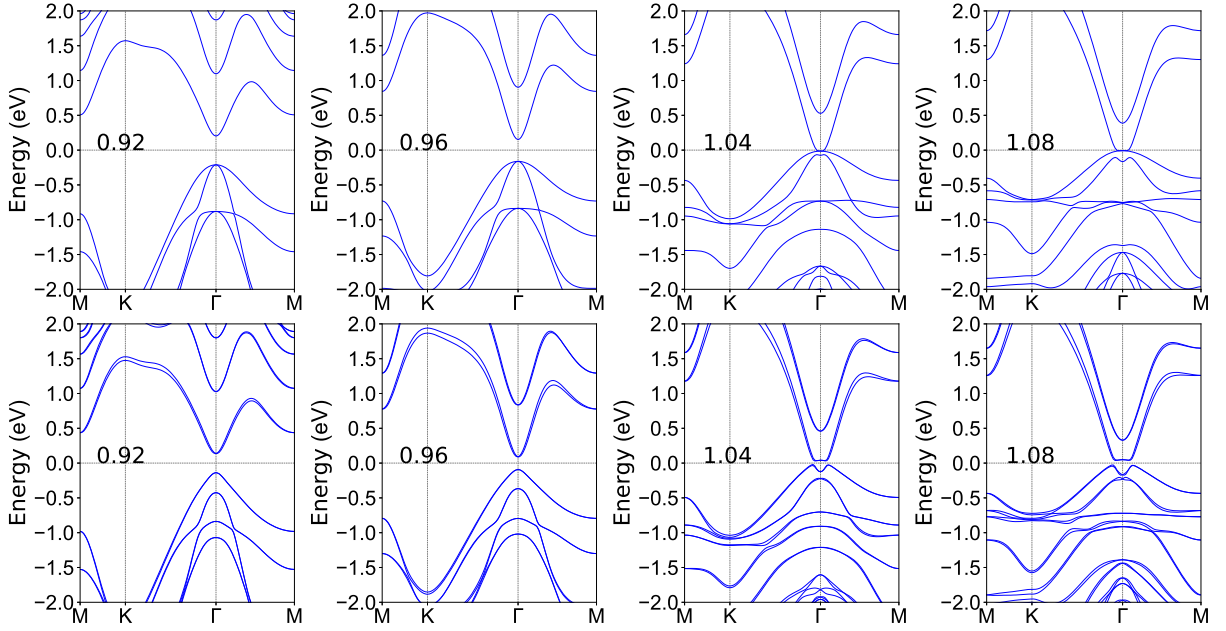


FIG. 4. (Color online) The energy band structures of SrAlGaSe₄ monolayer using GGA (Top) and GGA+SOC (Bottom) at representative 0.92, 0.94, 1.04 and 1.08 strains.

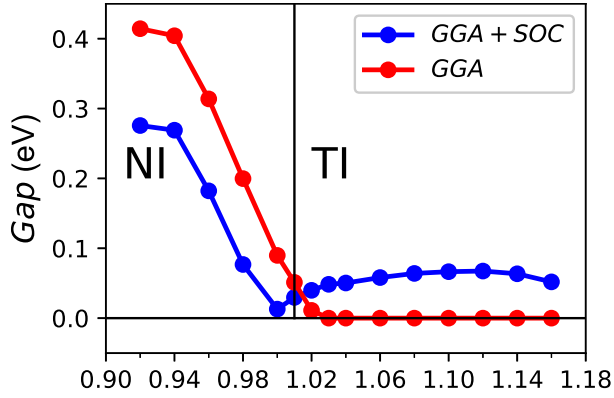


FIG. 5. (Color online) The energy band gaps of SrSiGeN₄ monolayer as a function of a/a_0 by using both GGA and GGA+SOC.

ing Voigt notation, the elastic tensor with hexagonal symmetry can be given:

$$C = \begin{pmatrix} C_{11} & C_{12} & 0 \\ C_{12} & C_{11} & 0 \\ 0 & 0 & (C_{11} - C_{12})/2 \end{pmatrix} \quad (1)$$

The two independent elastic constants of monolayer SrAlGaSe₄ are $C_{11}=82.67 \text{ Nm}^{-1}$ and $C_{12}=30.14 \text{ Nm}^{-1}$. The shear modulus is $G^{2D}=26.27 \text{ Nm}^{-1}$, which can be attained by $(C_{11}-C_{12})/2$, namely C_{66} . The calculated C_{11} and C_{66} satisfy the Born criteria of mechanical stability of a material with hexagonal symmetry⁵¹: $C_{11}>0$ and $C_{66}>0$, which confirms the mechanical stability of monolayer SrAlGaSe₄. The Young's modulus C_{2D} are

given⁵²:

$$C_{2D} = \frac{C_{11}^2 - C_{12}^2}{C_{11}} \quad (2)$$

The calculated C_{2D} is 71.68 Nm^{-1} , which are very smaller than ones of monolayer MSi₂N₄ (M=Ti, Zr, Hf, Cr, Mo and W) and Janus MSiGeN₄ (M=Mo and W)^{15,49}, indicating that monolayer SrAlGaSe₄ is not rigid. The Poisson's ratio ν is also calculated by C_{12}/C_{11} , and it is 0.37. The phonon calculations, AIMD and elastic constants show dynamical, thermal and mechanical stability of the monolayer SrAlGaSe₄, suggesting its possible synthesis.

IV. ELECTRONIC STRUCTURES

With GGA and GGA+SOC, the energy bands of monolayer SrAlGaSe₄ are shown in Figure 3. The GGA results show that the monolayer SrAlGaSe₄ is direct gap semiconductor (89.8 meV) with the valence band maximum (VBM) and conduction band minimum (CBM) being at the Γ point. When including SOC, an indirect gap of 12.9 meV is observed, and the CBM still locates at Γ point, but the VBM deviates slightly from Γ point. The other SOC effects are that the Rashba spin splitting near the CBM and the spin-orbit splitting of 209 meV at VBM are observed. It is found that the conduction and valence bands near the Fermi level are mainly s and p dominated ones, respectively. It has been proved that monolayer SrGa₂Se₄ is a 2D TI by using GGA³⁴. In order to ascertain the topological properties in the

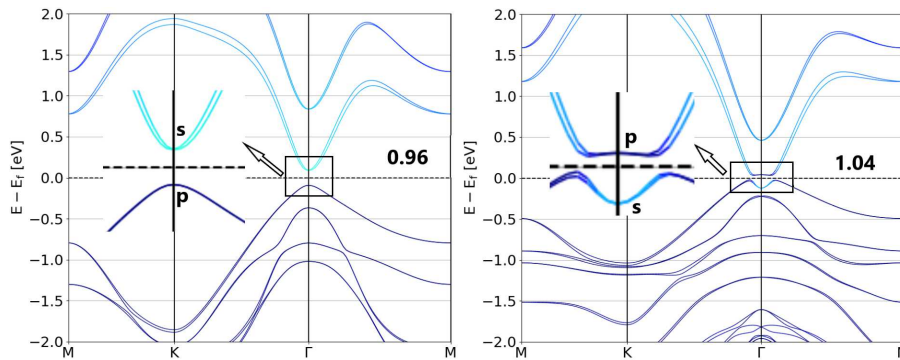


FIG. 6. (Color online) The s and p orbital projected band structures of SrAlGaSe₄ monolayer by using GGA+SOC at 0.96 and 1.04 strains.

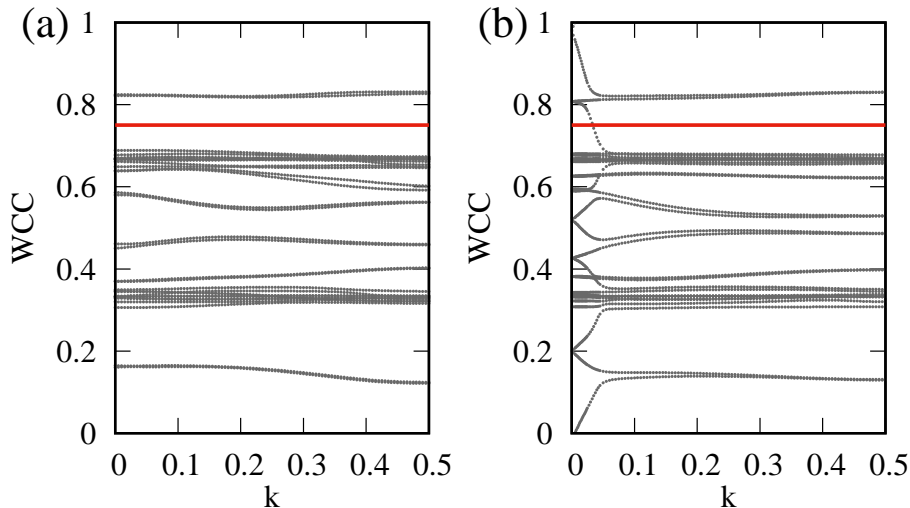


FIG. 7. (Color online) Evolution of WCC of SrAlGaSe₄ monolayer at 0.96 (a) and 1.04 (b) strains. The $Z_2=0$ at 0.96 strain for topological trivial feature and $Z_2=1$ at 1.04 strain for topological non-trivial one.

monolayer SrAlGaSe₄, we calculate the Z_2 topological invariants, which can be confirmed via calculations of the Wannier charge center (WCC). If Z_2 equals 1, a material is a topologically nontrivial state, and $Z_2 = 0$ means a trivial state. According to WCC in Figure 3, it is clearly seen that the number of crossings between the WCC and the reference horizontal line is even, which means that monolayer SrAlGaSe₄ is NI.

To achieve PQSHI, a strategy should be used to realize topological state in monolayer SrAlGaSe₄. Although monolayer SrGa₂Se₄ and SrAl₂Se₄ have the same configuration of outer shell electrons, the SrGa₂Se₄ is TI, while SrAl₂Se₄ is NI³⁴. The possible reason is that SrGa₂Se₄ has larger lattice constants than SrAl₂Se₄. The lattice constants of SrAlGaSe₄ is between ones of monolayer SrGa₂Se₄ and SrAl₂Se₄. So, it is possible to achieve topologically nontrivial state in monolayer SrAlGaSe₄ by strain engineering. Similar idea has been used in monolayer BiSb and SbAs, and NI to TI transition can be induced by biaxial tensile strain^{53,54}. Here, we use a/a_0 to simulate compressive/tensile strain with a and a_0 be-

ing the strained and unstrained lattice constants, respectively. The $a/a_0 < 1/a/a_0 > 1$ means compressive/tensile strain. The strain range from 0.90 to 1.16 is considered to calculate the electronic structures of SrAlGaSe₄ monolayer. The energy bands at representative strain points are plotted in Figure 4 with both GGA and GGA+SOC, and the energy band gaps of both GGA and GGA+SOC as a/a_0 function are shown in Figure 5. From 0.90 to 1.03 strain, the GGA gap decreases, and then the GGA gap is always zero from 1.03 to 1.16 strain. When including SOC, the SOC effect opens gap from 1.03 to 1.16 strain, which suggests that monolayer SrAlGaSe₄ may become potential 2D TI. However, we calculate Z_2 at all strain points to confirm critical point of NI to TI, and it is about at 1.01, which means that very small tensile strain can induce NI to TI transition.

To further understand the NI and TI, the s and p orbital projected band structures of SrAlGaSe₄ monolayer by using GGA+SOC at 0.96 and 1.04 strains are plotted in Figure 6. At 0.96 strain, the CBM of SrAlGaSe₄ at Γ point comprises with s -dominated orbitals, and its

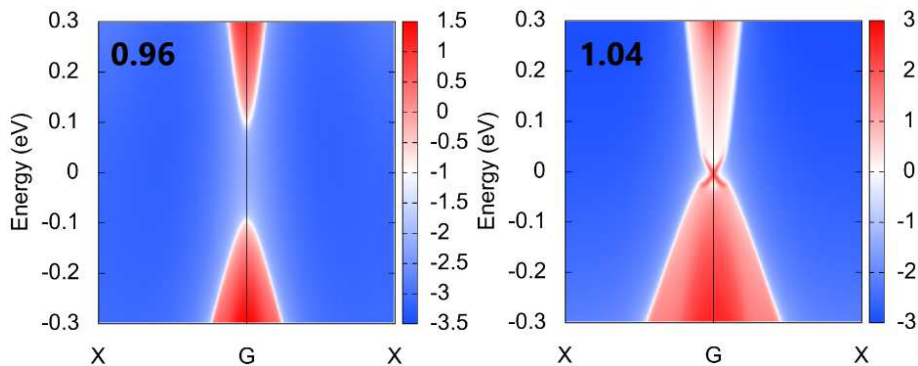


FIG. 8. (Color online) The edge states of semi-infinite SrAlGaSe₄ under 0.96 and 1.04 strains.

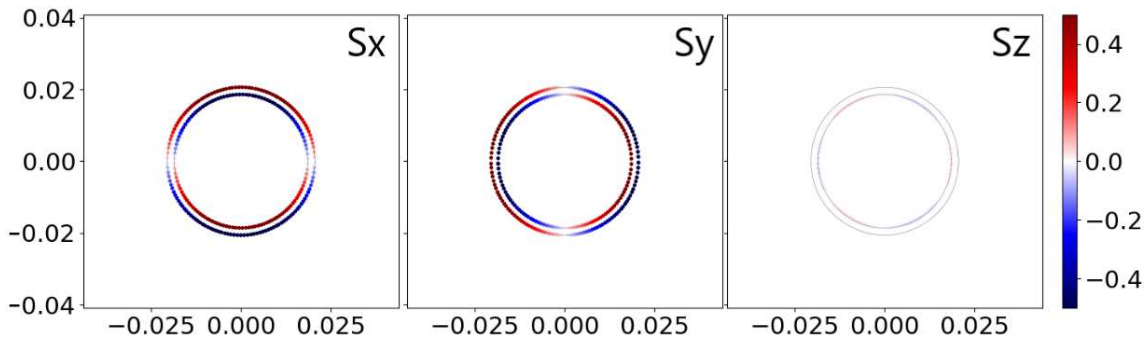


FIG. 9. (Color online) Spin texture calculated in $k_z = 0$ plane centered at the Γ point at the iso-energy surface of 0.2 eV above the Fermi level for SrAlGaSe₄ monolayer. The red and blue colours show spin-up and spin-down states, respectively.

VBM consists of p -dominated orbitals. In contrast, at 1.04 strain, an opposite situation is observed, and the conduction bands near the Fermi level around Γ point have the p -dominated orbitals, whereas the valence bands now become s -dominated orbitals, which means the occurrence of the electronic band inversion, implying the possible topological non-trivial feature. Figure 7 shows the WCCs of 0.96 and 1.04 strained SrAlGaSe₄ monolayers. For an arbitrary horizontal reference line (e.g. WCC=0.75), it crosses the evolution of WCC even number at 0.96 strain and odd number at 1.04 strain, respectively. In other words, the SrAlGaSe₄ monolayer at 0.96 strain is a trivial NI with $Z_2=0$, while under 1.04 tensile strain it transforms to a TI with $Z_2=1$. Furthermore, a TI has to exhibit non-trivial topological edge states. The Green's-function method is used to calculate the surface states on (100) surface based on the tight-binding Hamiltonian, which are plotted in Figure 8 at 0.96 and 1.04 strains. For the trivial NI under 0.96 compressive strain, no edge states are observed. In contrast, for the TI under 1.04 tensile strain, topological helical edge states with the appearance of the Dirac cone is observed, which connect the conduction and valence bands.

Coexistence of intrinsic piezoelectricity and nontrivial band topology (namely PQSHI) in monolayer SrAlGaSe₄ has been achieved by strain. Moreover, the Rashba spin splitting can exist in PQSHT due to the breaking of vertical reflection symmetry. To examine the Rashba ef-

fect, the in-plane spin-texture of monolayer SrAlGaSe₄ is calculated. The spin projected constant energy contour plots (0.2 eV above the Fermi level) of the spin textures calculated in k_x - k_y plane centered at the Γ point are shown in Figure 9. For both S_x and S_y spin components, the pair of spin-splitting bands have opposite spin orientation. The concentric spin-texture circles mean the purely 2D Rashba spin splitting at the conduction bands near the Fermi level. According to the projection of different spin components, the only in-plane S_x and S_y spin components are present in the Rashba spin split bands, while out-of-plane S_z component disappears. The in-plane spin moments at the two rings have opposite chirality with clockwise for the large ring and anticlockwise for the small ring, respectively.

V. PIEZOELECTRIC PROPERTIES

A noncentrosymmetric material with applied strain or stress will induce electric dipole moments, which can produce an electrical voltage. The pristine SrGa₂Se₄ monolayer is non-piezoelectric due to having centrosymmetry. However, monolayer SrAlGaSe₄ with particular Janus structure will possess piezoelectric effect. The piezoelectric response of a material can be described by third-rank piezoelectric stress tensor e_{ijk} and strain tensor d_{ijk} , which from the sum of ionic and electronic contributions

are defined as:

$$e_{ijk} = \frac{\partial P_i}{\partial \varepsilon_{jk}} = e_{ijk}^{elc} + e_{ijk}^{ion} \quad (3)$$

and

$$d_{ijk} = \frac{\partial P_i}{\partial \sigma_{jk}} = d_{ijk}^{elc} + d_{ijk}^{ion} \quad (4)$$

In which P_i , ε_{jk} and σ_{jk} are polarization vector, strain and stress, respectively. The superscripts *elc* and *ion* mean electronic and ionic contributions with $e_{ijk}^{elc}/d_{ijk}^{elc}$ (e_{ijk}/d_{ijk}) being clamped-ion (relax-ion) piezoelectric coefficients. The e_{ijk} and d_{ijk} can be related by elastic tensor C_{mnjk} :

$$e_{ijk} = \frac{\partial P_i}{\partial \varepsilon_{jk}} = \frac{\partial P_i}{\partial \sigma_{mn}} \cdot \frac{\partial \sigma_{mn}}{\partial \varepsilon_{jk}} = d_{imn} C_{mnjk} \quad (5)$$

For 2D materials, only the in-plane strain and stress are taken into account (namely $\varepsilon_{jk}=\sigma_{ij}=0$ for $i=3$ or $j=3$)^{8,13}. Due to a $3m$ point-group symmetry for monolayer SrAlGaSe₄, the piezoelectric stress and strain tensors by using Voigt notation can be reduced into :

$$e = \begin{pmatrix} e_{11} & -e_{11} & 0 \\ 0 & 0 & -e_{11} \\ e_{31} & e_{31} & 0 \end{pmatrix} \quad (6)$$

$$d = \begin{pmatrix} d_{11} & -d_{11} & 0 \\ 0 & 0 & -2d_{11} \\ d_{31} & d_{31} & 0 \end{pmatrix} \quad (7)$$

When a uniaxial in-plane strain is applied, monolayer SrAlGaSe₄ has both in-plane and vertical piezoelectric polarization ($e_{11}/d_{11} \neq 0$ and $e_{31}/d_{31} \neq 0$). However, when the biaxial in-plane strain is applied, the in-plane piezoelectric response will be suppressed, while the out-of-plane one still will remain ($e_{11}/d_{11}=0$ and $e_{31}/d_{31} \neq 0$). The e_{ij} can be calculated by DFPT, and the d_{ij} can be derived by Equation 1, Equation 5, Equation 6 and Equation 7:

$$d_{11} = \frac{e_{11}}{C_{11} - C_{12}} \quad \text{and} \quad d_{31} = \frac{e_{31}}{C_{11} + C_{12}} \quad (8)$$

Here, we investigate the piezoelectric properties of monolayer SrAlGaSe₄ with 1.06 strain as a representative TI. Firstly, the C_{11} and C_{12} are calculated with GGA by SSR, and they are 54.14 Nm⁻¹ and 23.30 Nm⁻¹, which are smaller than ones of unstrained SrAlGaSe₄ monolayer. Tensile strain reduced C_{11} and C_{12} have been found in many 2D materials^{49,55}. And then, we use the orthorhombic supercell as the computational cell (in Figure 1) to calculate e_{ij} with GGA+SOC by DFPT. The e_{ij} of monolayer SrAlGaSe₄ are calculated, and the calculated in-plane e_{11} and out-of-plane e_{31} are -0.575×10^{-10} C/m and -0.053×10^{-10} C/m. Based on Equation 8, the calculated d_{11} and d_{31} are -1.865 pm/V and -0.068 pm/V. So, the monolayer SrAlGaSe₄ can become a potential PQSHI by strain.

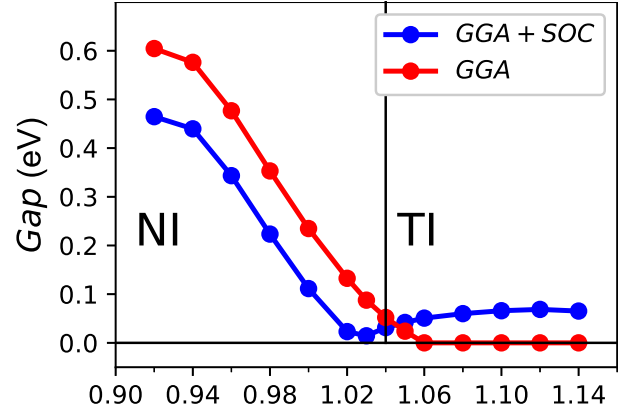


FIG. 10. (Color online) The energy band gap of CaSiGeN₄ monolayer as a function of a/a_0 by using both GGA and GGA+SOC.

VI. DISCUSSIONS AND CONCLUSION

For MoSi₂N₄ monolayer, the HSE06 (GGA) gives an indirect gap semiconductor with the gap of 2.297 (1.744) eV, and the experimental value is 1.94 eV³³. The difference between HSE06 (GGA) and experimental value is 0.357 (-0.196) eV. So, it may be more suitable for MA₂Z₄ family to use GGA to study their electronic properties. Although the GGA may underestimate energy gap of monolayer SrAlGaSe₄, our predicted PQSHI should be qualitatively correct, and only the critical point of NI to TI phase transition changes. The focus of our works is to provide a idea to achieve PQSHI, and many PQSHIs should be constructed in MA₂Z₄ family. To confirm that, we also investigate the NI to TI phase transition of CaAlGaSe₄ monolayer caused by strain. The optimized lattice constants is 4.02 Å, and the calculated C_{11} and C_{12} are 89.95 Nm⁻¹ and 30.71 Nm⁻¹, which satisfy the Born criteria of mechanical stability⁵¹. The dynamical stability is also proved by phonon band dispersions of CaAlGaSe₄ monolayer from Fig.1 of electronic supplementary information (ESI), and the thermal stability is confirmed from Fig.2 of ESI. The energy band gaps of both GGA and GGA+SOC as a/a_0 function are shown in Figure 10, and the energy bands at representative strain points are plotted in Fig.3 of ESI. It is found that the transition point of NI to TI is about 1.04, which is larger than one of SrAlGaSe₄. The evolution of WCC and edge states of CaAlGaSe₄ monolayer at representative 1.06 strain are shown in Fig.4 and Fig.5 of ESI, which clearly show the nontrivial band topology. At representative 1.06 strain, the calculated in-plane e_{11} and out-of-plane e_{31} are 3.071×10^{-10} C/m and -0.066×10^{-10} C/m. Based on Equation 8, the calculated d_{11} and d_{31} are 8.07 pm/V and -0.077 pm/V with C_{11} and C_{12} being 61.59 Nm⁻¹ and 23.52 Nm⁻¹. These show that CaAlGaSe₄ monolayer can become PQSHI by tensile strain.

In summary, our DFT calculations demonstrate that it is possible to realize piezoelectricity and robust non-

trivial band topology in a single material. The electronic structure of Janus monolayer SrAlGaSe₄ with piezoelectric properties at very small strain can act as a prototype for designing PQSHI. Moreover, the PQSHI can coexist with Rashba spin splitting due to lacking vertical reflection symmetry. Most importantly, many PQSHIs can be achieved in 2D MA₂Z₄ family by using the same design principle of SrAlGaSe₄ monolayer, for example Janus CaAlGaSe₄ monolayer. The realization of PQSHI with Rashba spin splitting can potentially lead to new device applications in electronics and spintronics, and can stimulate further studies for multifunctional 2D materials.

ACKNOWLEDGMENTS

This work is supported by the Natural Science Foundation of Shaanxi Provincial Department of Education (19JK0809). We are grateful to the Advanced Analysis and Computation Center of China University of Mining and Technology (CUMT) for the award of CPU hours and WIEN2k/VASP software to accomplish this work.

-
- ¹ J. H. Yang, A. P. Wang, S. Z. Zhang, J. Liu, Z. C. Zhong and L. Chen, *Phys. Chem. Chem. Phys.*, **21**, 132 (2019).
 - ² S. D. Guo, W. Q. Mu, Y. T. Zhu and X. Q. Chen, *Phys. Chem. Chem. Phys.* **22**, 28359 (2020).
 - ³ Y. D. Ma, L. Z. Kou, B. B. Huang, Y. Dai and T. Heine, *Phys. Rev. B* **98**, 085420 (2018).
 - ⁴ J. W. Huang, X. Duan, S. Jeon, Y. Kim, J. Zhou, J. Li and S. Liu, arXiv:2101.07980 (2021).
 - ⁵ C. W. Niu, H. Wang, N. Mao, B. B. Huang, Y. Mokrousov and Y. Dai, *Phys. Rev. Lett.* **124**, 066401 (2020).
 - ⁶ W. Wu and Z. L. Wang, *Nat. Rev. Mater.* **1**, 16031 (2016).
 - ⁷ C. F. Wang, H. J. Li, M. G. Li et al., *Adv. Funct. Mater.* **315**, 2009457 (2021).
 - ⁸ K. N. Duerloo, M. T. Ong and E. J. Reed, *J. Phys. Chem. Lett.* **3**, 2871 (2012).
 - ⁹ W. Wu, L. Wang, Y. Li, F. Zhang, L. Lin, S. Niu, D. Chenet, X. Zhang, Y. Hao, T. F. Heinz, J. Hone and Z. L. Wang, *Nature* **514**, 470 (2014).
 - ¹⁰ H. Zhu, Y. Wang, J. Xiao, M. Liu, S. Xiong, Z. J. Wong, Z. Ye, Y. Ye, X. Yin and X. Zhang, *Nat. Nanotechnol.* **10**, 151 (2015).
 - ¹¹ L. Dong, J. Lou and V. B. Shenoy, *ACS Nano*, **11**, 8242 (2017).
 - ¹² R. X. Fei, We. B. Li, J. Li and L. Yang, *Appl. Phys. Lett.* **107**, 173104 (2015).
 - ¹³ M. N. Blonsky, H. L. Zhuang, A. K. Singh and R. G. Hennig, *ACS Nano*, **9**, 9885 (2015).
 - ¹⁴ Y. Chen, J. Y. Liu, J. B. Yu, Y. G. Guo and Q. Sun, *Phys. Chem. Chem. Phys.* **21**, 1207 (2019).
 - ¹⁵ S. D. Guo, Y. T. Zhu, W. Q. Mu and W. C. Ren, *EPL* **132**, 57002 (2020).
 - ¹⁶ Y. Guo, S. Zhou, Y. Z. Bai, and J. J. Zhao, *Appl. Phys. Lett.* **110**, 163102 (2017).
 - ¹⁷ S. D. Guo, Y. T. Zhu, W. Q. Mu, L. Wang and X. Q. Chen, *Comp. Mater. Sci.* **188**, 110223 (2021)
 - ¹⁸ W. B. Li and J. Li, *Nano Res.* **8**, 3796 (2015).
 - ¹⁹ H. Rostami, F. Guinea, M. Polini, R. Roldán, *npj 2D Materials and Applications* **2**, 1 (2018).
 - ²⁰ V. Shahnazaryan, H. Rostami, arXiv:2012.13730 (2020).
 - ²¹ M. Z. Hasan and C. L. Kane, *Rev. Mod. Phys.* **82**, 3045 (2010).
 - ²² X. L. Qi and S. C. Zhang, *Rev. Mod. Phys.* **83**, 1057 (2011).
 - ²³ C. L. Kane and E. J. Mele, *Phys. Rev. Lett.* **95**, 226801 (2005).
 - ²⁴ M. König, S. Wiedmann, C. Brune et al., *Science* **318**, 766 (2007).
 - ²⁵ I. Knez, R. R. Du and G. Sullivan, *Phys. Rev. Lett.* **107**, 136603 (2011).
 - ²⁶ C. C. Liu, W. Feng, Y. Yao, *Phys. Rev. Lett.* **107**, 076802 (2011).
 - ²⁷ S. Zhou, C. C. Liu, J. J. Zhao and Y. G. Yao, *npj Quant. Mater.* **3**, 16 (2018).
 - ²⁸ S. Murakami, *Phys. Rev. Lett.* **97**, 236805 (2006).
 - ²⁹ J. J. Zhou, W. X. Feng, C. C. Liu, S. Guan and Y. G. Yao, *Nano Lett.* **14**, 4767 (2014).
 - ³⁰ Y. Xu, B. Yan, H. J. Zhang et al., *Phys. Rev. Lett.* **111**, 136804 (2013).
 - ³¹ H. M. Weng, X. Dai and Z. Fang, *Phys. Rev. X* **4**, 011002 (2014).
 - ³² S. D. Guo, W. Q. Mu, Y. T. Zhu, S. Q. Wang and G. Z. Wang, arXiv:2101.11942 (2021).
 - ³³ Y. L. Hong, Z. B. Liu, L. Wang T. Y. Zhou, W. Ma, C. Xu, S. Feng, L. Chen, M. L. Chen, D. M. Sun, X. Q. Chen, H. M. Cheng and W. C. Ren, *Science* **369**, 670 (2020).
 - ³⁴ L. Wang, Y. P. Shi, M. F. Liu et al., arXiv:2008.02981 (2020).
 - ³⁵ S. Li, W. K. Wu, X. L. Feng et al., *Phys. Rev. B* **102**, 235435 (2020).
 - ³⁶ J. H. Yu, J. Zhou, X. G. Wan, Q. F. Li, arXiv:2012.14120 (2020).
 - ³⁷ C. Yang, Z. G. Song, X. T. Sun and J. Lu, *Phys. Rev. B* **103**, 035308 (2021).
 - ³⁸ L. M. Cao, G. H. Zhou, Q. Q. Wang, L. K. Ang and Y. S. Ang, *Appl. Phys. Lett.* **118**, 013106 (2021).
 - ³⁹ P. Hohenberg and W. Kohn, *Phys. Rev.* **136**, B864 (1964); W. Kohn and L. J. Sham, *Phys. Rev.* **140**, A1133 (1965).
 - ⁴⁰ G. Kresse, *J. Non-Cryst. Solids* **193**, 222 (1995).
 - ⁴¹ G. Kresse and J. Furthmüller, *Comput. Mater. Sci.* **6**, **15** (1996).
 - ⁴² G. Kresse and D. Joubert, *Phys. Rev. B* **59**, 1758 (1999).
 - ⁴³ J. P. Perdew, K. Burke and M. Ernzerhof, *Phys. Rev. Lett.* **77**, 3865 (1996).
 - ⁴⁴ U. Herath, P. Tavazde, X. He, E. Bousquet, S. Singh, F. Munoz and A. H. Romero, *Computer Physics Communications* **251**, 107080 (2020).
 - ⁴⁵ A. Togo, F. Oba, and I. Tanaka, *Phys. Rev. B* **78**, 134106 (2008).
 - ⁴⁶ X. Wu, D. Vanderbilt and D. R. Hamann, *Phys. Rev. B* **72**, 035105 (2005).
 - ⁴⁷ Q. Wu, S. Zhang, H. F. Song, M. Troyer and A. A. Soluyanov, *Comput. Phys. Commun.* **224**, 405 (2018).
 - ⁴⁸ A. A. Mostofia, J. R. Yatesb, G. Pizzif, Y.-S. Lee, I.

- Souzad, D. Vanderbilte and N. Marzarif, *Comput. Phys. Commun.* **185**, 2309 (2014).
- ⁴⁹ S. D. Guo, W. Q. Mu, Y. T. Zhu, R. Y. Han and W. C. Ren, *J. Mater. Chem. C*, 2021, DOI: 10.1039/D0TC05649A.
- ⁵⁰ S. D. Guo, X. S. Guo, R. Y. Han and Y. Deng, *Phys. Chem. Chem. Phys.* **21**, 24620 (2019).
- ⁵¹ R. C. Andrew, R. E. Mapasha, A. M. Ukpong and N. Chetty, *Phys. Rev. B* **85**, 125428 (2012).
- ⁵² E. Cadelano, P. L. Palla, S. Giordano and L. Colombo, *Phys. Rev. B* **82**, 235414 (2010).
- ⁵³ S. L. Zhang, M. Q. Xie, B. Cai, H. J. Zhang, Y. D. Ma, Z. F. Chen, Z. Zhu, Z. Y. Hu, and H. B. Zeng, *Phys. Rev. B* **93**, 245303 (2016).
- ⁵⁴ W. Y. Yu, C. Y. Niu, Z. L. Zhu et al., *RSC Adv.* **7**, 27816 (2017).
- ⁵⁵ S. D. Guo, W. Q. Mu and Y. T. Zhu, *J. Phys. Chem. Solids* **151**, 109896 (2021).